# High-order amplitude equation for steps on the creep curve

Mulugeta Bekele[1,*] and G. Ananthakrishna[2]
[1]*Department of Physics, Indian Institute of Science, Bangalore 560 012, India*
[2]*Materials Research Centre, Indian Institute of Science, Bangalore 560 012, India*
(Received 5 May 1997; revised manuscript received 21 July 1997)

We consider a model proposed by one of the authors for a type of plastic instability found in creep experiments which reproduces a number of experimentally observed features. The model consists of three coupled nonlinear differential equations describing the evolution of three types of dislocations. The transition to the instability has been shown to be via Hopf bifurcation, leading to limit cycle solutions with respect to physically relevant drive parameters. Here we use a reductive perturbative method to extract an amplitude equation of up to *seventh* order to obtain an approximate analytic expression for the order parameter. The analysis also enables us to obtain the bifurcation (phase) diagram of the instability. We find that while supercritical bifurcation dominates the major part of the instability region, subcritical bifurcation gradually takes over at *one end* of the region. These results are compared with the known experimental results. Approximate analytic expressions for the limit cycles for different types of bifurcations are shown to agree with their corresponding numerical solutions of the equations describing the model. The analysis also shows that high-order nonlinearities are important in the problem. This approach further allows us to map the theoretical parameters to the experimentally observed macroscopic quantities. [S1063-651X(97)12011-6]

PACS number(s): 62.20.Hg, 05.45.+b, 81.40.Lm, 83.50.By

## I. INTRODUCTION

Instabilities in plastic flow have been an object of attention for a long time in metallurgical literature. Experimentally, there are basically three modes of deformation of a specimen. The best known and mostly widely studied form of the instability arises when the specimen is subjected to a constant rate of tensile deformation commonly referred to as the constant strain rate test [1,2]. Clearly, this method of deformation is conceptually difficult to understand since the specimen is subjected to a predetermined response (i.e., a constant rate of deformation), and the force or the stress developed in the sample is sought to be measured. Under normal conditions, one finds a smooth stress-strain curve. However, when the system is in the regime of instability (i.e., for some values of the material parameters), the stress-strain curve exhibits repeated load drops. Each of the load drops is associated with the formation and propagation of dislocation bands [3]. There is another form of testing, where the deformation is carried out keeping the stress rate fixed. Again, under normal conditions one finds a smooth stress-strain curve. However, when the material is deformed in the instability regime of the parameter space, one finds a stepped response in the stress-strain curve. This method of deformation is equally popular among experimentalists for the study of the instability. However, conceptually the simplest form of the instability [4] manifests itself when the material is subjected to a creep test wherein a force is applied and the response in the form of elongation of the specimen is measured. Here again, under normal conditions, the strain-time curve is smooth. Under certain metallurgical conditions, one sees steps on the creep curve suggesting a form of instability [4,5]. It is in the former two types of testing that the plastic instability manifests much more easily than in the last case, and hence these two modes of deformation are usually adopted. In contrast, the phenomenon of steps on a creep curve, which is the subject of the present discussion, is seen in much fewer instances [5,6]. Instabilities occurring in all these forms are considered to be of common origin. The phenomenon is referred to as the Portevin–Le Chatelier (PLC) effect or the jerky flow, and is seen in several metals such as commercial aluminium, brass, on alloys of aluminium and magnesium [1]. In the case of the constant strain rate case, it is observed only in a window of strain rates and temperature.

It is generally agreed that the microscopic origin of the instabilities arises due to the interaction of dislocations with mobile point defects, and is referred to as dynamic strain aging. This leads to negative strain rate characteristic of the flow stress. The basic idea was formulated by Cottrell [7] a few decades ago. Early phenomenological models, including Cottrell's theory and its extensions [7,8], do not deal with time development. In contrast, techniques of dynamical systems address precisely this aspect. Recently, there has been a resurgence of interest in plastic instabilities [9–13] in light of the introduction of new methodology borrowed from the theory of dynamical systems. This has helped to obtain insights hitherto not possible [10–20] One of the aims of such theories is to be able to relate the microscopic dislocation mechanisms to the measurable macroscopic quantities.

An attempt to understand the problem in the above perspective was made by Ananthakrishna and co-workers several years ago [12,13]. The basic idea was to describe the problem from the point of view of a far-from-equilibrium transition, wherein the new temporal order could be described as a cooperative phenomenon [21,22]. In a series of papers [23,24], starting from an extended Fokker-Planck equation for the velocity of dislocation segments, these au-

*On leave from Department of Physics, Addis Ababa University, Addis Ababa, Ethiopia.

 

thors arrived at a model which consisted of three types of dislocations and some transformations between them [12]. The basic idea could be summarized by stating that limit cycle solutions arise due to nonlinear interaction between three different types of dislocations, suggesting a new mathematical mechanism for the instability. Even though the spatial inhomogeneous structure was ignored and only the temporal oscillatory state was sought to be described, the model and its extensions to the case of constant strain rate test [13], proved to be very successful in that it could explain most of the experimentally observed features such as the existence of bounds on strain rate for the PLC effect to occur, the negative strain rate sensitivity, etc. [2,7,13]. One other important prediction, which is a direct consequence of the dynamical basis of the model, is the existence of chaotic stress drops in a range of strain rates [14,15]. *Recently, there have been several attempts which verify this prediction* [17-20]. *Indeed this verification suggests that these few modes represent the collective degrees of freedom of dislocations*. (Note that the spatially extended nature of the system implies infinite degrees of freedom.) From this point of view, dealing with the temporal aspect appears to be justified. A description of the phenomenon which includes the initiation and propagation of the bands during the PLC effect has also been recently attempted [16].

Since the introduction of bifurcation theory into this field several years ago by our group [12,13], several other groups have also undertaken similar lines of attack [9–12,25]. In the process, we feel that finer aspects of dynamical systems have been glossed over in this field. For instance, one often finds that casual remarks are made about fast and slow modes without actually going through the procedure of demonstrating the existence of such modes and eliminating the fast modes in favor of the slow ones [25]. In addition, under the adiabatic elimination, the resulting modes which serve as order parameter variables are very complicated functions of the original modes. Yet, hand waiving arguments have been used in building models which we believe are technically suspect.

In our recent work [26] we showed how, under certain conditions, one of the variables of the model could be adiabatically eliminated since the time constant of this mode can be chosen to be much faster than the other two (i.e., for low values of a parameter $b_0$, see below). We then derived the equation for the order parameter of the reduced model. We found both supercritical and subcritical bifurcation within the range of applicability. We also found that the results were in good agreement both with the reported experimental results and with the numerical solution of the model. However, eliminating one of the variables entirely restricts the applicability of the analysis to the two-dimensional plane of the parameter space (parameters $a$ and $c$; see below). In addition, we also found that even within the limited domain, very high-order nonlinearities control most of the bifurcation domain.

The purpose of the present work is to perform the analysis by keeping all the three modes in the model, and to explore the entire instability domain spanned by all the three parameters ($a$, $b_0$, and $c$). In addition, this analysis should help us to verify if high-order nonlinearities could control part of the subcritical bifurcation, as found in our recent analysis [26]. This will help us to investigate the full nature of the bifurcation in detail. We use the reductive perturbative method and extract a complex order parameter which is directly related to the amplitude and the frequency of the jumps on the creep curve. The analysis should also help us to compare the results with the experimental ones. The expression for the order parameter is checked by comparing it with the numerical solution of the model.

In what follows (Sec. II) we present a brief summary of the model. In Sec. III we use the reductive perturbative method to extract the amplitude equation up to *seventh* (septic) order. This enables us not only to determine the nature of bifurcation (i.e., supercritical or subcritical) exhibited by the model, but also gives us an expression for the order parameter over most of the instability domain. In Sec. IV, the approximate limit cycle solution obtained through the amplitude equation is compared with the experimental results as well as with the numerical solution of the model. Section V contains summary and discusses our results.

## II. MODEL FOR STEPS ON CREEP CURVE

We start with a brief summary of the model. The details of the model can be found in the original references [12]. The model consists of mobile dislocations, immobile dislocations, and another type which mimics Cottrell-type dislocations, which are dislocations with clouds of solute atoms. Let the corresponding densities be $N_m$, $N_{im}$, and $N_i$, respectively. The rate equations for the densities of dislocations are

$$\frac{dN_m}{dt} = \theta V_m N_m - \beta N_m^2 - \beta N_m N_{im} + \gamma N_{im} - \alpha_m N_m , \quad (1)$$

$$\frac{dN_{im}}{dt} = \beta N_m^2 - \beta N_{im} N_m - \gamma N_{im} + \alpha_i N_i , \quad (2)$$

$$\frac{dN_i}{dt} = \alpha_m N_m - \alpha_i N_i . \quad (3)$$

The first term in Eq. (1) is the rate of production of dislocations due to cross glide with a rate constant $\theta V_m$, where $V_m$ is the velocity of the mobile dislocations, which in general depends on some power of the applied stress, $\sigma_a$. The second term refers to two mobile dislocations either annihilating or immobilizing. The third term also represents the annihilation of a mobile dislocation with an immobile one. The fourth term represents the remobilization of the immobile dislocations due to stress or thermal activation [see $\gamma N_{im}$ in Eq. (2)]. The last term represents the immobilization of mobile dislocations either due to solute atoms or due to other pinning centers. $\alpha_m$ refers to the concentration of the solute atoms which participate in slowing down the mobile dislocations. Once a mobile dislocation starts acquiring solute atoms, we regard it as a new type of dislocation, namely Cottrell's type $N_i$. This process is represented as an incoming term in Eq. (3). As they acquire more and more solute atoms they will slow down and eventually stop the dislocation entirely. At this point, they are considered to have transformed to $N_{im}$. This process is represented by a loss term in Eq. (3) and a gain term in Eq. (2). These equations can be cast into a dimensionless form by using scaled variables

$$x=N_m\left(\frac{\beta}{\gamma}\right),\quad y=N_{im}\left(\frac{\beta}{\theta V_m}\right),\quad z=N_i\left(\frac{\beta\alpha_i}{\gamma\alpha_m}\right),\quad \tau=\theta V_m t \tag{4}$$

to obtain

$$\dot{x}=(1-a)x-b_0x^2-xy+y, \tag{5}$$

$$\dot{y}=b_0(b_0x^2-xy-y+az), \tag{6}$$

$$\dot{z}=c(x-z), \tag{7}$$

where the dot represents differentiation with respect to $\tau$, while $a=\alpha_m/\theta V_m$, $b_0=\gamma/\theta V_m$, and $c=\alpha_i/\theta V_m$. Equations (5)–(7) are coupled set of nonlinear equations which support limit cycle solutions for a range of parameters $a$, $b_0$, and $c$ that are physically relevant. $a$ refers to the concentration of the solute atoms, $b_0$ refers to the reactivation of immobile dislocations, and $c$ to the time scales over which the slowing down occurs. The dependence on stress and temperature appears through $V_m$. We demonstrated the existence of limit cycle solutions and also obtained approximate closed-form solutions for the limit cycles [12]. In addition, the model was studied numerically. Using the Orowan equation which relates the rate of change of strain ($\dot{S}$) to dislocation density and the mean velocity: $\dot{S}=bN_mV_m$, with $b$ as the Burger's vector, steps on the creep curve follow automatically, since the densities of dislocations are oscillatory. Several experimental results are reproduced [12].

### III. REDUCTIVE PERTURBATIVE APPROACH

We briefly outline the reductive perturbative approach to problems of formation of new states of order in far-from-equilibrium situations. Transitions occurring in these systems are quite analogous to equilibrium phase transitions. The general idea is to construct a ''potential-like function'' for the ''order-parameter''-like variable in the neighborhood of the critical value of the drive parameter. This would permit the use of the methods developed in equilibrium phase transitions for further analysis.

Near the point of Hopf bifurcation of the system [Eqs. (5)–(7)], corresponding to a value near the critical drive parameter, a pair of complex conjugate eigenvalues and another real negative eigenvalue exist for the linearized system of equations around the steady state. As we approach the critical value from the stable side, the real part of the pair of complex conjugate eigenvalues approaches zero from the negative side, and hence the corresponding eigendirections have a slow time scale. As we enter the instability region, these real parts become positive. In contrast, the effect of the change in the drive parameter on the real negative eigenvalue is negligible. Thus, *while the two eigenvectors corresponding to the pair of complex conjugate eigenvalues are slow modes, the eigenvector corresponding to the real negative eigenvalue is a fast (and decaying) mode*. For this reason, the slow modes determine the formation of new states of order. *The reductive perturbative method is a method where the slow enslaving dynamics is extracted in a systematic way* [27-32]. The method involves first finding the critical eigenvectors corresponding to the bifurcation point and expressing the general solution as a linear combination of these vectors. The effect of the nonlinearity is handled progressively using the multiple-scale method. The equation governing the complex order parameter takes the form of the Stuart-Landau equation, and corresponds to the time-dependent Ginzburg-Landau equation (TDGL) for a homogeneous medium. (Henceforth, we will also refer to this equation as the amplitude equation.) On the other hand, the asymptotic solution, which is a limit cycle, collapses to the subspace spanned by the slow modes with no trace of the fast mode. It may be worth emphasizing that this method is essentially the same as reduction to the center manifold. Indeed, the equivalence of the center manifold theory [33–35] to the reductive perturbation has been established [32]. Other techniques of extracting amplitude equations have been devised whose end results are basically the same. For instance, a perturbative renormalization-group method [36,32], and its recent extension on the basis of envelope theory [37], has also been developed as a tool for a global asymptotic analysis which can be used to extract the amplitude equations.

We start with Eqs. (5)–(7). There is only one fixed point, defined by

$$x_a=z_a=\frac{1-2a+[(1-2a)^2+8b_0]^{1/2}}{4b_0}\quad\text{and}\quad y_a=\frac{1}{2}. \tag{8}$$

Defining new variables which are deviations from the fixed point

$$X=x-x_a,\quad Y=y-y_a,\quad\text{and}\quad Z=z-z_a, \tag{9}$$

Eqs. (5)–(7) become

$$\dot{X}=-(\alpha X+\chi Y+b_0X^2+XY), \tag{10}$$

$$\dot{Y}=-b_0(\Gamma X+\delta Y-aZ-b_0X^2+XY), \tag{11}$$

$$\dot{Z}=c(X-Z), \tag{12}$$

where

$$\alpha=a+2b_0x_a+y_a-1,\quad \chi=x_a-1,$$
$$\Gamma=y_a-2b_0x_a,\quad \delta=x_a+1. \tag{13}$$

Equations (10)–(12) will be solved reductive perturbatively. [We note here that it is possible to reduce this system of equations to only two by adiabatically eliminating Eq. (10). This is done by noting that, when $b_0$ and $c$ are much smaller than $a$, by rescaling Eq. (10), it can be shown to be fast variable and hence can be adiabatically eliminated. This was what was done in Ref. [26].] Writing these equations as a matrix equation where the nonlinear part appears separately from the linear part, we obtain

$$\frac{d\vec{R}}{d\tau}=\mathbf{L}\vec{R}+\vec{N}, \tag{14}$$

where

$$\vec{R}=\begin{pmatrix} X \\ Y \\ Z \end{pmatrix}, \tag{15}$$

$$\mathbf{L}=\begin{pmatrix} -\alpha & -\chi & 0 \\ -b_0\Gamma & -b_0\delta & ab_0 \\ c & 0 & -c \end{pmatrix}, \tag{16}$$

and the nonlinear part $\vec{N}$ is given by

$$\vec{N}=\begin{pmatrix} -b_0X^2-XY \\ b_0(b_0X^2-XY) \\ 0 \end{pmatrix}. \tag{17}$$

Consider the stability of the fixed point as a function of the parameter $c$. The eigenvalues $\lambda_i$, $i=1$, 0, and $-1$, of the matrix $\mathbf{L}$ are determined from the cubic equation

$$\lambda^3-T\lambda^2+P\lambda-\Delta=0, \tag{18}$$

where

$$T=-(\alpha+\delta b_0+c), \tag{19}$$

$$P=\delta b_0 c+\alpha(\delta b_0+c)-\chi\Gamma b_0, \tag{20}$$

and

$$\Delta=-b_0c[\alpha\delta+\chi(a-\Gamma)]. \tag{21}$$

The fixed point becomes unstable when one of the following conditions are violated [38]:

$$T<0,\Delta<0 \quad \text{or} \quad \Delta-PT>0. \tag{22}$$

It is easy to show that the first two inequalities are not violated. Substituting for $\Delta$, $P$, and $T$ in the third inequality of Eq. (22), we obtain

$$(\alpha+\delta b_0)c^2+[(\alpha+\delta b_0)^2-\chi a b_0]c + b_0(\alpha+\delta b_0)(\alpha\delta-\chi\Gamma)<0 \tag{23}$$

as the condition for instability. Using the equality sign in Eq. (23) gives us the critical value of the drive parameter, $c=c_0$, for given values of $a$ and $b_0$. For $c<c_0$, the fixed point is unstable. Since $c$ is non-negative (negative $c$ is unphysical), we obtain a unique $c_0$ for the allowed pair of $a$ and $b_0$ values within the instability. Figure 1 shows a three-dimensional plot of the instability region involving all the three parameters of the model. (Note that since all the variables and the parameters are dimensionless quantities, we have plotted all figures in dimensionless quantities.)

To obtain an approximate analytical solution of Eq. (14), we follow a reductive perturbative approach similar to that used in Refs. [30] and [31]. We choose $c=c_0(1-\epsilon)$ with $0<\epsilon\ll 1$, and write the matrix $\mathbf{L}$ as a sum of two matrices, $\mathbf{L}=\mathbf{L}_0+\epsilon\mathbf{L}_1$, where $\mathbf{L}_0$ is the matrix $\mathbf{L}$ evaluated for $c=c_0$, and

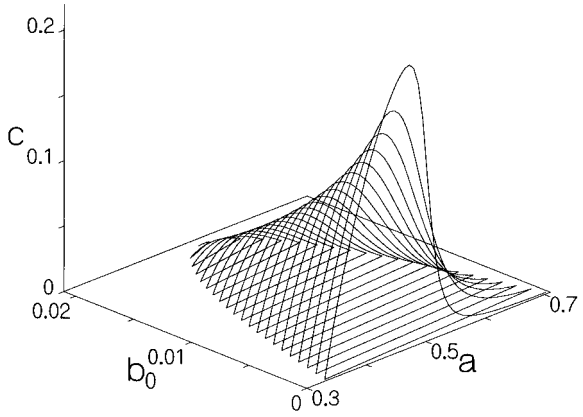


FIG. 1. The instability region determined by all the three independent parameters $a$, $b_0$, and $c$ of the model. It is bounded by the three surfaces: the $c_0$ surface (shown by a series of curved lines), the $c=0$ plane (shown by a series of straight lines), and the $b_0=0$ plane. [Note that the $c_0$ surface is determined from Eq. (23).]

$$\mathbf{L}_1\equiv\begin{pmatrix} 0 & 0 & 0 \\ 0 & 0 & 0 \\ -c_0 & 0 & c_0 \end{pmatrix}. \tag{24}$$

The eigenvalues of $\mathbf{L}_0$ are

$$\lambda_{1,-1}=\pm\imath\omega \quad \text{and} \quad \lambda_0=T, \tag{25}$$

where $\omega^2=P$ ($P$ and $T$ being evaluated at $c=c_0$). Taking the solution for $\vec{R}$ as a growth out of the critical eigenmodes, we express it as a linear combination of these eigenmodes:

$$\vec{R}(\tau)=\Psi\, e^{\imath\omega\tau}\vec{r}_1+\Psi_0 e^{\lambda_0\tau}\vec{r}_0+\Psi^* e^{-\imath\omega\tau}\vec{r}_1^{\,*}=\sum_{j=1}^{-1}\Psi_j e^{\lambda_j\tau}\vec{r}_j \tag{26}$$

where $\vec{r}_j$'s are right eigenvectors defined by $\mathbf{L}_0\vec{r}_j=\lambda_j\vec{r}_j$ with $\vec{r}_{-1}=\vec{r}_1^{\,*}$. We also introduce left eigenvectors, $\vec{s}_j^{\,T}$, defined by $\vec{s}_j^{\,T}\mathbf{L}_0=\lambda_j\vec{s}_j^{\,T}$, where $T$ stands for the transpose. Substituting this expression for $\vec{R}$ in the matrix equation, Eq. (14), and multiplying both sides of the equation by one of the left eigenvectors, we obtain an equation governing the corresponding amplitude:

$$e^{\lambda_j\tau}\,\frac{d\Psi_j}{d\tau}=\epsilon\sum_k \mu_{jk}\Psi_k e^{\lambda_k\tau}+\sum_{l,m\,,m\le l} g_{jlm}\Psi_l\Psi_m e^{(\lambda_l+\lambda_m)\tau}. \tag{27}$$

Expressions for the coefficients $\mu_{jk}$ and $g_{jlm}$ are given in Eq. (C11) and Eqs. (C13) and (C14), respectively, in Appendix C.

We express $\Psi_j$ as a power series expansion in $\epsilon^{1/2}$:

$$\Psi_j=\epsilon^{1/2}\psi_j^{(1)}+\epsilon\psi_j^{(2)}+\epsilon^{3/2}\psi_j^{(3)}+\cdots, \tag{28}$$

and introduce multiple time scales such that

$$\frac{d}{d\tau}=\frac{\partial}{\partial\tau}+\epsilon\frac{\partial}{\partial\tau_1}+\epsilon^2\frac{\partial}{\partial\tau_2}+\cdots, \tag{29}$$

where $\tau_1=\epsilon\tau$, $\tau_2=\epsilon^2\tau$, . . . . Substituting these expressions for $\Psi_j$ and $d/d\tau$ into the equation for the amplitudes, Eq. (27), we successively solve by equating terms of the same order in powers of $\epsilon$. First, terms of $\mathcal{O}(\epsilon^{1/2})$ give

$$\frac{\partial\psi_j^{(1)}}{\partial\tau}=0, \tag{30}$$

implying that $\psi_j^{(1)}$ is constant in the time scale of $\tau$. $O(\epsilon)$ terms give the equation

$$\frac{\partial\psi_j^{(2)}}{\partial\tau}=\sum_{k,l,l\leqslant k} g_{jkl}\psi_k^{(1)}\psi_l^{(1)}e^{(\lambda_k+\lambda_l-\lambda_j)\tau}, \tag{31}$$

which, upon integration, gives

$$\psi_j^{(2)}e^{\lambda_j\tau}=\sum_{k,l,\ l\leqslant k} h_{jkl}\psi_k^{(1)}\psi_l^{(1)}e^{(\lambda_k+\lambda_l)\tau}, \tag{32}$$

where $h_{jkl}=g_{jkl}/(\lambda_k+\lambda_l-\lambda_j)$. $\mathcal{O}(\epsilon^{3/2})$ terms give the equation

$$\frac{\partial\psi_j^{(3)}}{\partial\tau}+\frac{\partial\psi_j^{(1)}}{\partial\tau_1}=\sum_k \mu_{jk}\psi_k^{(1)}e^{(\lambda_k-\lambda_j)\tau}+\sum_{k,l,,l\leqslant k} g_{jkl}(\psi_k^{(1)}\psi_l^{(2)} + \psi_k^{(2)}\psi_l^{(1)})e^{(\lambda_k+\lambda_l-\lambda_j)\tau}. \tag{33}$$

Using the compatibility condition, we match terms that are varying on a slow time scale found on both sides of the equality, and extract the slow dynamics

$$\frac{\partial\psi_j^{(1)}}{\partial\tau_1}=\mu_{jj}\psi_j^{(1)}+\eta_j|\psi_1^{(1)}|^2\psi_j^{(1)}. \tag{34}$$

An expression for $\eta_j$ is given in Eq. (C12) in Appendix C. Since we are interested in asymptotic solutions, the equations governing the oscillatory amplitude $\Psi$ and its complex conjugate $\Psi^*$ are our concern. (The subscript $j=1$ is left out from $\Psi_1$ for the sake of brevity.) To $\mathcal{O}(\epsilon^{1/2})$, $\Psi=\epsilon^{1/2}\psi^{(1)}$ and, thus, Eq. (27) takes the form of a *cubic* Stuart-Landau equation:

$$\frac{d\Psi}{d\tau}=\epsilon\mu\Psi+\eta|\Psi|^2\Psi. \tag{35}$$

Note that $\mu(=\mu_{11})\equiv\mu_r+\imath\mu_i$ and $\eta(=\eta_1)\equiv\eta_r+\imath\eta_i$ are complex coefficients. $\Psi$ is the complex order parameter variable whose steady-state solution gives its amplitude (squared) as

$$|\Psi|^2=-\epsilon\frac{\mu_r}{\eta_r}, \tag{36}$$

and its frequency $\Omega$ (with $\Psi=|\Psi|e^{\imath\Omega\tau}$) as

$$\Omega=\epsilon\left(\mu_i-\frac{\eta_i}{\eta_r}\mu_r\right). \tag{37}$$

This solution exists provided $\eta_r$ is negative since $\mu_r$ is positive. $\eta_r$ is found to be negative over a major part of the instability region in the $b_0-a$ plane, as shown in Fig. 2 (the unshaded region). In this case, since the amplitude of the order parameter grows continuously in proportion to $\epsilon^{1/2}$ [see Eq. (36)], the transition is continuous (a second-order-type transition) corresponding to supercritical bifurcation. There is a relatively small portion of the instability region, shown in the same figure in shades, where $\eta_r$ is found to be positive implying that the transition is discontinuous corresponding to subcritical bifurcation. In this regime, one has to go to quintic or even higher terms in the amplitude equation to obtain an expression for the order parameter. We carried out the reductive perturbative method further to derive the *quintic*,

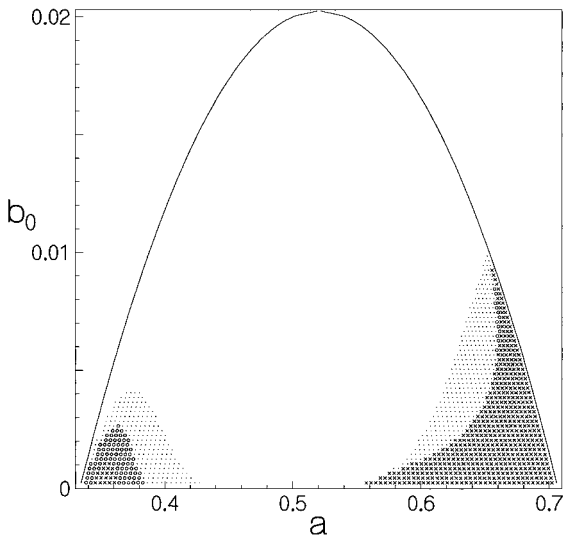


FIG. 2. Plot of the bifurcation diagram in the $a$-$b_0$ plane. The instability region is bounded by the parabolic-shaped curve and the $b_0=0$ line. The unshaded (shaded) region exhibits supercritical (subcritical) bifurcation. The shaded region marked by dots (open circles) shows the portion within the subcritical bifurcation, where the quintic (septic) amplitude equation is supposed to hold.

$$\frac{d}{d\tau}\Psi=\epsilon\mu\Psi+\eta|\Psi|^2\Psi+\nu|\Psi|^4\Psi, \tag{38}$$

as well as *septic*,

$$\frac{d}{d\tau}\Psi=\epsilon\mu\Psi+\eta|\Psi|^2\Psi+\nu|\Psi|^4\Psi+\xi|\Psi|^6\Psi, \tag{39}$$

amplitude equations. [Expressions for the complex coefficients $\nu=\nu_r+\imath\nu_i$ and $\xi=\xi_r+\imath\xi_i$ are given in Eqs. (A3) and (A4), respectively, in Appendix A.] The amplitude (squared), $|\Psi|^2$, and frequency, $\Omega$, found from the steady-state solution of the quintic amplitude equation, are

$$|\Psi|^2=\frac{1}{2}\left\{-\frac{\eta_r}{\nu_r}+\left[\left(\frac{\eta_r}{\nu_r}\right)^2-4\epsilon\frac{\mu_r}{\nu_r}\right]^{1/2}\right\}, \tag{40}$$

and

$$\Omega=\epsilon\mu_i+\eta_i|\Psi|^2+\nu_i|\Psi|^4, \tag{41}$$

while these same quantities found from the steady-state solution of the septic amplitude equation are

$$|\Psi|^2=\frac{1}{2}\left\{-\frac{\nu_r}{\xi_r}+\left[\left(\frac{\nu_r}{\xi_r}\right)^2-4\frac{\eta_r}{\xi_r}\right]^{1/2}+\epsilon\frac{\mu_r}{\eta_r}\right\}+\mathcal{O}(\epsilon^2) \tag{42}$$

and

$$\Omega=\epsilon\mu_i+\eta_i|\Psi|^2+\nu_i|\Psi|^4+\xi_i|\Psi|^6. \tag{43}$$

The ranges of validity of the quintic and septic amplitude equations enable us to describe a large portion of the subcritical bifurcation. Figure 2 also shows the portion within the subcritical bifurcation where the dynamics of the system is supposed to be governed by the *quintic* (marked by dots) and *septic* (marked by open circles) amplitude equations. The rest of the domain of subcritical bifurcation, where *even* higher-order amplitude equation need to be considered, is marked by crosses on the same figure.

As can be seen from Fig. 2, there are two distinct regions of subcritical bifurcation located on either side of $a=0.5$. The crossover from a supercritical to subcritical bifurcation is first seen for $b_0=0.01$ around $a=0.65$ as the value of $b_0$ is reduced. The extent of subcritical bifurcation in the $b_0-a$ plane increases as $b_0$ decreases. The validity of the amplitude equations will be examined by comparing the asymptotic solution derived from them with that of the limit cycle solution found by numerically integrating the model equations.

## IV. COMPARISON WITH EXPERIMENTS AND NUMERICAL SOLUTIONS

### A. Comparison with experiments

To start with, consider the supercritical regime, where expressions for the amplitude and period of the limit cycle are relatively simple. Using the steady-state solution of the cubic amplitude equation, Eqs. (36) and (37), the dependence of amplitude $|\Psi|^2$ and period $P$ $[\propto 1/(\omega+\Omega)]$, of the limit cycle on $a$ or $b_0$ can be obtained. (Here we will only consider how the two quantities $|\Psi|^2$ and $P$ depend on $b_0$ for fixed $a$. A similar analysis can be carried out for parameter $a$ fixing $b_0$.) The parameter $b_0(=\gamma/\theta V_m)$ is a function of the applied stress $(\sigma_a)$ and temperature $(T)$. As remarked earlier, $\gamma$ represents the stress and thermal activation, and, at temperatures of interest, thermal activation can be completely ignored. As for the stress activation, it is a threshold process and, therefore, can be taken to have a weak dependence on stress until a critical value of this stress, beyond which it should show a rapid increase. One such functional form for $\gamma$ could be $\exp(-\sigma_c/\sigma)$, where $\sigma_c$ represents the value of the stress beyond which the function rapidly rises. Since stress activation occurs at large values, one expects $\sigma_c$ to be large. Using the standard expression [39] for $V_m(\sigma_a,T)=V_0(\sigma_a/\sigma_0)^m\exp(-E_m/kT)$ (with $m>1$), we obtain

$$b_0\sim\gamma(\sigma)\left(\frac{\sigma_a}{\sigma_0}\right)^{-m}e^{E_m/kT}. \tag{44}$$

From this, we see that $b_0$ has a decreasing dependence on stress, with the term $(\sigma_a/\sigma_0)^{-m}$ dominating up to $\sigma_c$, beyond which it should increase. Clearly, $b_0$ decreases as a function of $T$. Figure 3 shows plots of $|\Psi|^2$ and $P$ as a function of $b_0$. From the above discussion on the dependence of $b_0$ on $\sigma$ and $T$, we see that $|\Psi|^2$ should increase as stress increases for the *major part* of the stress value, since $\sigma_c$ is large. On the other hand, it should decrease with an increase in temperature. Since stress and temperature are measurable quantities, our predictions can be compared with experimental results. The amplitude and period of the limit cycle are related, respectively, to the amount of strain jumps and the period of the jumps on the creep curve calculated through the Orowan equation. There are very few experiments in this mode of testing, as mentioned in Sec. I. The only experiment where this dependence on stress and temperature has been measured for a limited range is that in Ref. [5]. According to this, the amplitude of the strain jumps increases with stress while its period has a decreasing dependence on stress. Experiments from constant strain rate case also exhibit the same trend when the results are translated in terms of constant stress experiments. It is well known that the amplitude of the stress drops decreases with applied strain rate. In fact, even the numerical solution of the equations extended to the constant strain rate case predicts this behavior [13]. This implies that the amplitude of strain jumps should increase as stress increases [40]. [This relation can be seen as follows. In the constant strain rate case, the deformation rate is fixed, and the stress developed in the sample is measured. When the contribution to the plastic strain rate increases due to increased dislocation motion (for whatever reasons), the stress has to fall in order to keep the applied strain rate constant. Thus the relation between strain rate and stress is opposite.] Clearly, the general trend is consistent with the experimental results for most of the value of $b_0$. The authors of Ref. [5] also reported that the amplitude of the strain jumps increases while its period decreases with increase in temperature, which is consistent with our result.

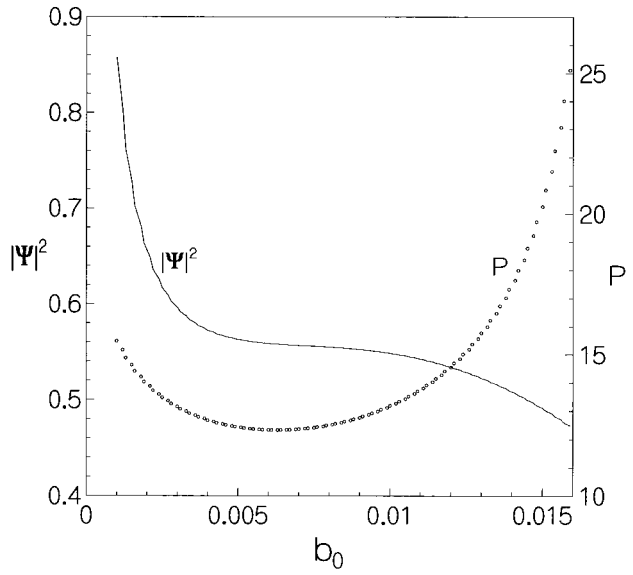


FIG. 3. Plots of $|\Psi|^2$ and $P$ vs $b_0$ within the supercritical domain, when $a=0.45$ and $\epsilon=0.01$.

Figure 4 shows plots of the amplitude (squared) and period of the limit cycle (LC) as a function of $b_0$ for a certain interval within the subcritical bifurcation. Using an analysis

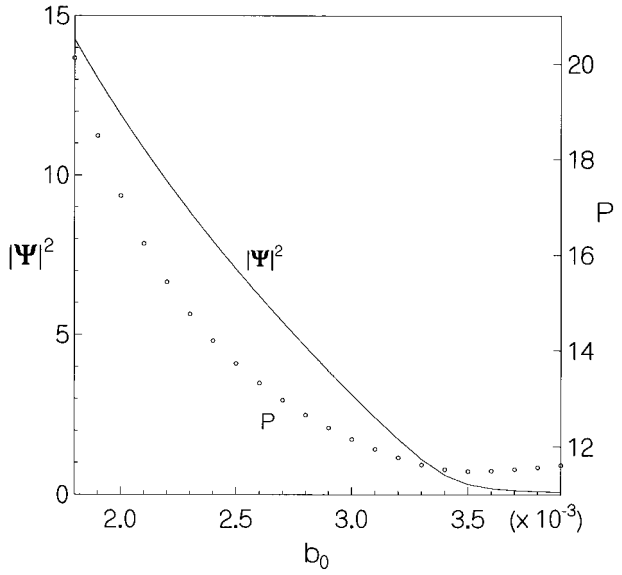


FIG. 4. Plots of $|\Psi|^2$ and $P$ vs $b_0$ within the subcritical domain when $a=0.39$ and $\epsilon=10^{-4}$.

similar to that above, we find that while the dependence of the amplitude on $b_0$ is consistent with the experimental results reported in Ref. [5], the dependence of the period on $b_0$ is predominantly inconsistent with this report.

Experiments in the constant strain rate case show that the stress drops are seen to arise both abruptly as well as continuously [10]. Translating this result to the constant stress case, it implies that the strain jumps can arise both abruptly and continuously. This feature is manifest in the supercritical and subcritical bifurcations seen in our calculations.

### B. Comparison with numerical solutions

Having derived the amplitude equation, we now compare its result with the numerical solutions obtained via Eqs. (10)–(12). As stated earlier, there are two distinct types of solutions, namely, the supercritical and the subcritical solutions. Even in the region of subcritical bifurcation, we have three types—first, where the quintic amplitude equation works; second, where the septic amplitude equation works; and, third, the rest of the instability domain where even higher-order nonlinearities dominate and, as such, require even higher-order amplitude equations. We will compare the solutions obtained from these with the numerically exact solutions of Eqs. (10)–(12).

First consider the supercritical region. Using the steady-state solution of the cubic amplitude equation, Eqs. (36) and (37), in Eq. (26) leads to an analytic expression for the LC near bifurcation points in the domain of supercritical bifurcation. This is usually referred to as the *secular equation*. The derivation of the equations governing the LC are given in Appendix B. This solution can be compared with the numerically exact solution obtained by integrating the system of equations, Eqs. (10)–(12). Since the region of applicability in the $b_0-a$ plane is large, we choose one solution for large values of $b_0$ (at the top end of the bifurcation diagram) and another value of $b_0$ at the lower end. Figures 5(a) and 5(b) show the plots of the secular equation along with their respective numerical solutions for two widely spaced transition points within the domain of supercritical bifurcation. As can be observed clearly, they match very well.

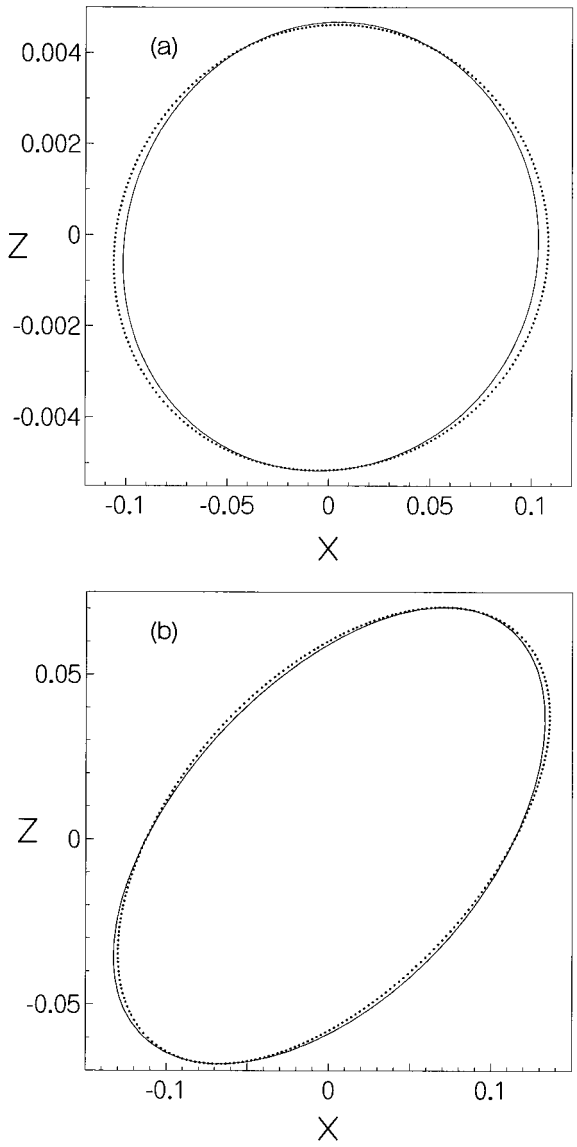


FIG. 5. Plots of the limit cycle solutions (in the $X$-$Z$ plane) obtained from the secular equation (solid line) and that obtained from numerical integration of the model [Eqs. (10)–(12)] (marked with dots) when (a) $a=0.521$, $b_0=0.0202$, and $\epsilon=0.1$, and when (b) $a=0.6$, $b_0=0.01$, and $\epsilon=0.001$. Both bifurcation points lie within the supercritical bifurcation domain.

In a manner similar to the supercritical bifurcation, the analytic expression for the LC for a *large portion of the domain of the subcritical bifurcation* is obtained by using the steady-state solution of the quintic or septic amplitude equations. In this case, there are three distinct types of solutions: (a) first, where $\nu_r$ is negative and $\xi_r$ positive, implying that only the quintic amplitude equation has a steady-state solution; (b) second, when $\nu_r$ and $\xi_r$ are both negative implying that both the quintic and septic amplitude equations support steady-state solutions; and (c) third, when $\nu_r$ is positive and $\xi_r$ is negative, implying that the septic amplitude equation supports a steady-state solution while the quintic does not. The resulting LC's are compared with those found from the numerical ones. For case (a), we picked two different bifur-

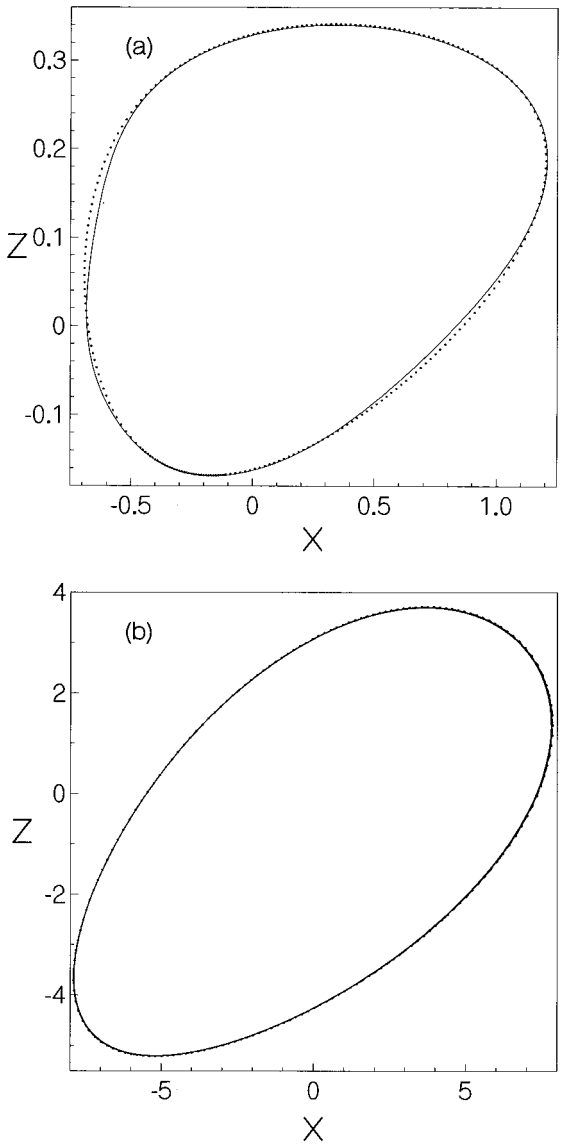


FIG. 6. Plots of the limit cycle solutions (in the $X$-$Z$ plane) obtained from the secular equation (solid line) and that obtained from numerical integration of the model [Eqs. (10)–(12c)] (marked with dots) when (a) $a=0.647$, $b_0=0.009$ and $\epsilon=0.01$ and when (b) $a=0.38$, $b_0=0.004$, and $\epsilon=0.0001$. Both bifurcation points lie within the subcritical bifurcation domain where the quintic amplitude equation holds (i.e., $\nu_r<0$ and $\xi_r>0$).

cation points—one to the right and another to the left of $a=0.5$. Plots in Figs. 6(a) and 6(b) show LC's, obtained from the secular equation and from numerical equations. For case (b), Fig. 7 shows three plots of LC's, two of which are obtained from the secular equations corresponding to the quintic and septic amplitude equations, while the third one is obtained from the numerical solution. It is clear from this figure that the LC derived from the septic amplitude equation is a better approximation than that derived from the quintic one. This shows that the ''containing'' role is played not only by the quintic but also by the septic (and even higher) term of the nonlinearity. We also find that the region over which such a situation is valid is a substantial portion of the validity of the quintic amplitude equation, suggesting that higher-order nonlinearities are in fact important, as was indicated by our earlier work [26]. We show case (c) in Fig. 8, comparing the LC derived from the septic amplitude equation with that of the numerical one for a bifurcation point where the quintic amplitude equation *does not* hold. The agreement is reasonable except around the sharp turning point.

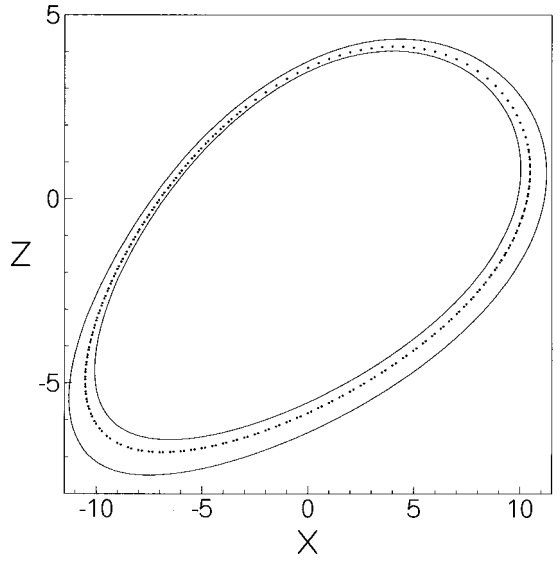


FIG. 7. Plots of the limit cycle solution (in the $X$-$Z$ plane) obtained by using the secular equation derived from the quintic amplitude equation (outer solid line), from the septic amplitude equation (inner solid line) and that obtained from numerical integration of the model [Eqs. (10)–(12)] (marked with dots) when $a=0.375$, $b_0=0.004$ and $\epsilon=0.0001$. The bifurcation point lies within the subcritical bifurcation domain, where *both* $\nu_r$ and $\xi_r$ are negative.

Finally, it is worthwhile to state that expansion of the amplitude equation even up to septic term fails to cover the

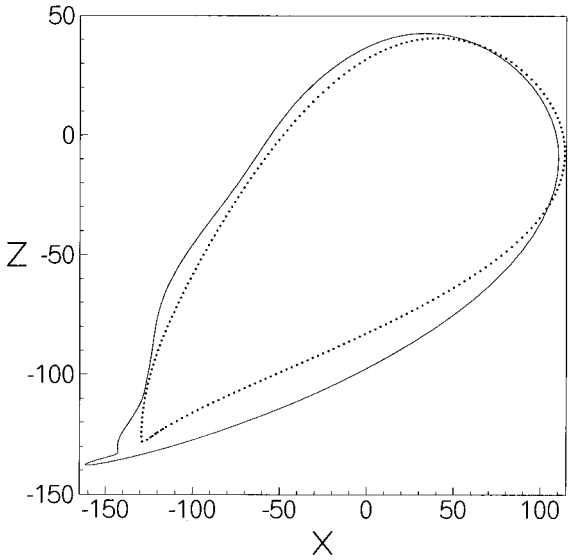


FIG. 8. Plots of the limit cycle solution (in the $X$-$Z$ plane) obtained from the secular equation (solid line), and that obtained from numerical integration of the model [Eqs. (10)–(12)] (marked with dots) when $a=0.37$, $b_0=0.001$, and $\epsilon=0.0001$. The bifurcation point lies within the subcritical bifurcation domain where $\nu_r>0$ and $\xi_r<0$.

entire instability domain, even though most of it is covered. This also suggests that higher-order nonlinearities control the rest of the subcritical bifurcation domain. This feature is not usually encountered in model systems.

The above comparison reveals the following: (i) The expression for the LC in the supercritical domain mimics the numerical solution very well, provided $\epsilon$ is taken to be small enough. (ii) In the subcritical domain, the two results also generally match well with each other. However, for values of the parameters where the value of $c$ is close to zero (which also corresponds to small values of $b_0$), higher-order nonlinearities could supplement the contributions arising from the lower ones in determining the LC. In other words, if the coefficient of the next-higher order has also a negative real part, its contribution may have to be included in the expression for the order parameter.

## V. SUMMARY AND DISCUSSION

We have carried out a reductive perturbative approach to the problem of steps on the creep curve, regarding it as a formation of ordered state when the system is driven away from equilibrium. The dynamics of the system is described by two coupled amplitude equations: one for a transient order parameter $\Psi_0$, and another for the complex order parameter $\Psi$ in the neighborhood of the bifurcation point. The order parameter $\Psi$ represents both the amplitude and the phase of the limit cycle solution when $\epsilon>0$. Since the above derivation is valid only in the neighborhood of the critical value, the expression for the order parameter $\Psi$ is valid only for small $\epsilon$. This has been exemplified by the quite reasonable agreements between the LC solutions found from the analytic expression and that from the numerical integration of the model. We have shown that both supercritical and subcritical bifurcations are seen in the transitions to the instability domain. *While the major part of the phase boundary exhibits supercritical bifurcation, subcritical bifurcation gradually dominates as the value of $b_0$ is reduced*. The results of an earlier calculation [12] which used the method of relaxation oscillation and showed a first-order-type transition, is consistent with the present one since the values of the parameters ($a=0.63$, $b_0=10^{-4}$) falls in the subcritical bifurcation domain. In our more recent work [26], where we first adiabatically eliminated one of the variables and then applied the reductive perturbative method for the reduced model, we found both supercritical and subcritical regions. However, due to the fact the adiabatic elimination itself was valid only for small values of $b_0$, the results were found to be valid in a small domain. Further, we found that very high-order nonlinearities were important. This result is supported by the present calculation.

The present analysis shows a feature which is normally not seen in model systems, namely, that higher-order terms than quintic may control the subcritical bifurcation. In fact, even when the quintic term plays the containing role, higher-order terms may also contribute significantly to the role of containment. Thus, in deriving the expression for the LC, it may be necessary to find out how higher- and higher-order nonlinear terms in the expansions in the amplitude equation contribute to the asymptotic solution.

We comment here on the unusual feature of the model in the context of phase transitions. For conventional models, in the language of phase transitions, the free energy is described by an expansion in power series of the order parameter up to sixth power. While the free energy for second-order phase transitions can be described by retaining up to fourth power in the order parameter, it is usually sufficient to retain the sixth power for the description of first-order phase transitions (with the appropriate signs for the coefficients in the expansion). In the present case, however, we need to go to as high as the eighth power (or more) of the order parameter in some regions of the drive parameter to describe the corresponding free energy when the transition is of first-order type. This feature is rather unusual, and not found in conventional models of phase transitions.

Due to the closed-form expressions for the order parameter, the present calculation helps us to map the theoretically introduced parameters to the experimentally measured quantities. *For instance, in experiments, one measures the amplitude of the strain jumps on the creep curve as well as their frequency as a function of stress and temperature. The dependence of the amplitude of the strain jumps and its frequency on stress and temperature can be evaluated by using the order parameter equations in Orowan's equation by noting that $|\Psi|$ corresponds to the amplitude of the strain jumps while the frequency $\Omega$* together with *$\omega$ gives a measure of the frequency of the steps*. By properly relating the parameter $b_0$ to stress and temperature, we found that for a certain range of the instability the amplitude increases while the period decreases as stress increases (at constant temperature), qualitatively agreeing with the reported experimental result of Ref. [5]. Also, the amplitude increases while the period decreases as temperature is increased (at constant stress) which is again consistent with the experimental results of Ref. [5]. In addition, we found other ranges within the instability showing various kinds of dependence of the order parameter on stress and temperature.

Finally, the present exercise demonstrated the complicated dependence of the order parameter variable on the original modes. This will serve as a warning to those using hand waiving arguments for declaring certain modes as fast modes and others as slow modes in the modeling of such problems.

## ACKNOWLEDGMENTS

One of us (M.B.) would like to thank the International Program in Physical Sciences, Uppsala University (Sweden) for offering a fellowship to study at Indian Institute of Science. This work was partially supported by IFCPAR Project No. 1108-1.

## APPENDIX A

In this appendix we give expressions for the coefficients appearing in the TDGL equation, i.e., expressions for $\mu$, $\eta$, $\nu$, and $\xi$ in the equation $(d/d\tau)\Psi=\epsilon\mu\psi+\eta|\Psi|^2\Psi+\nu|\Psi|^4\Psi+\xi|\Psi|^6\Psi$. Note that they are functions of the parameters $a$, $b_0$, and $c$. They are given below:

$$\mu=\mu_{11}, \tag{A1}$$

$$\eta=\sum_{k\leqslant\alpha\leqslant j,\,\gamma\leqslant\beta}(g_{1j\alpha}h_{j\beta\gamma}+g_{1\alpha k}h_{k\beta\gamma}). \tag{A2}$$

In Eq. (A2) and all the following equations, summations over *latin* alphabets run over 1, 0, and -1 while those over *Greek* alphabets run over $\pm 1$. A summation of Eq. (A2) includes only those terms which satisfy the condition $\alpha+\beta+\gamma=1$,

$$\nu=\sum_{k\leqslant j}(T_{jk}^{(1,4)}+T_{jk}^{(2,3)}), \tag{A3}$$

where

$$T_{jk}^{(1,4)}=\sum_{\zeta\leqslant\delta\leqslant\gamma\leqslant\beta\leqslant\alpha}(g_{1j\alpha}u_{j\beta\gamma\delta\zeta}+g_{1\alpha k}u_{k\beta\gamma\delta\zeta}) \tag{A4}$$

and

$$T_{jk}^{(2,3)}=\sum_{\beta\leqslant\alpha,\zeta\leqslant\delta\leqslant\gamma}(h_{j\alpha\beta}t_{k\gamma\delta\zeta}+h_{k\alpha\beta}t_{j\gamma\delta\zeta}), \tag{A5}$$

with the condition on the summations of Eqs. (A4) and (A5) to be $\alpha+\beta+\gamma+\delta+\zeta=1$. Finally, the septic coefficient $\xi$ is given by

$$\xi=\sum_{k\leqslant j}(T_{jk}^{(1,6)}+T_{jk}^{(2,5)}+T_{jk}^{(3,4)}), \tag{A6}$$

where

$$T_{jk}^{(1,6)}=\sum_{k\leqslant\alpha\leqslant j,\sigma\leqslant\rho\leqslant\zeta\leqslant\delta\leqslant\gamma\leqslant\beta\leqslant\alpha}(g_{1j\alpha}w_{j\beta\gamma\delta\zeta\rho\sigma}+g_{1\alpha k}w_{k\beta\gamma\delta\zeta\rho\sigma}), \tag{A7}$$

$$T_{jk}^{2,5}=\sum_{\beta\leqslant\alpha,\sigma\leqslant\rho\leqslant\zeta\leqslant\delta\leqslant\beta\leqslant\alpha}g_{1jk}(h_{j\alpha\beta}v_{k\gamma\delta\zeta\rho\sigma}+h_{k\alpha\beta}v_{j\gamma\delta\zeta\rho\sigma}), \tag{A8}$$

and

$$T_{jk}^{3,4}=\sum_{\gamma\leqslant\beta\leqslant\alpha,\sigma\leqslant\rho\leqslant\zeta\leqslant\delta}g_{1jk}(t_{j\alpha\beta\gamma}u_{k\delta\zeta\rho\sigma}+t_{k\alpha\beta\gamma}u_{j\delta\zeta\rho\sigma}), \tag{A9}$$

with the constraint $\alpha+\beta+\gamma+\delta+\zeta+\rho+\sigma=1$ imposed on the summations of Eqs. (A9), (A10), and (A11). Expressions for $\mu_{jk}$, $g_{jkl}$, $h_{jkl}$, $t_{jklm}$, $u_{jklmn}$, $v_{jklmnp}$, and $w_{jklmnpq}$ are given in Appendix C.

## APPENDIX B

In this appendix, an (approximate) asymptotic solution for $\vec{R}$ describing the limit cycle will be derived using the steady-state solution of the particular TDGL equation. For the instability region where the cubic TDGL equation holds, expansion of $\Psi$ up to $\psi_j^{(2)}$ will be involved in determining $\vec{R}$, so that

$$\vec{R}=\epsilon\psi_0^{(2)}e^{\lambda_o\tau}\vec{r}_0+[(\epsilon^{1/2}\psi^{(1)}+\epsilon\psi^{(2)})e^{iw\tau}\vec{r}+\text{c.c.}]. \tag{B1}$$

Note that the asymptotic solution does not contain the $\psi_0^{(1)}e^{\lambda_0\tau}$ term since, $\lambda_0$ being negative, it decays in time. To $\mathcal{O}(\epsilon^{1/2})$,

$$\Psi=\epsilon^{1/2}\psi^{(1)}\Rightarrow\psi^{(1)}=\epsilon^{-1/2}\Psi. \tag{B2}$$

Using Eqs. (B2) and (32) in Eq. (B1) will enable us to derive the components of $\vec{R}$, which are given by

$$X=A_x|\Psi|\cos(\Omega_c\tau+\theta_x)+B_{1x}|\Psi|^2\cos(2\Omega_c\tau+\phi_x)+B_{2x}|\Psi|^2+B_{3x}|\Psi|^2\cos(2\Omega_c\tau+\varphi_x), \tag{B3}$$

$$Y=A_y|\Psi|\cos(\Omega_c\tau+\theta_y)+B_{1y}|\Psi|^2\cos(2\Omega_c\tau+\phi_y)+B_{2y}|\Psi|^2+B_{3y}|\Psi|^2\cos(2\Omega_c\tau+\varphi_y), \tag{B4}$$

and

$$Z=A_z|\Psi|\cos(\Omega_c\tau+\theta_z)+B_{1z}|\Psi|^2\cos(2\Omega_c\tau+\phi_z)+B_{2z}|\Psi|^2+B_{3z}|\Psi|^2\cos(2\Omega_c\tau+\varphi_z), \tag{B5}$$

where

$$\Omega_c=\Omega+\omega, \tag{B6}$$

$$A_d=2|r_{1d}|, \tag{B7}$$

$$\theta_d=\sin^{-1}\left(\frac{\text{Im}(r_{1d})}{|r_{1d}|}\right), \tag{B8}$$

$$B_{1d}=2|h_{111}r_{1d}|, \tag{B9}$$

$$\phi_d=\sin^{-1}\left(\frac{\text{Im}(h_{111}r_{1d})}{|h_{111}r_{1d}|}\right), \tag{B10}$$

$$B_{2d}=2|h_{11-1}r_{1d}|, \tag{B11}$$

$$B_{3d}=2|h_{1-1-1}r_{1d}|, \tag{B12}$$

and

$$\varphi_d=\sin^{-1}\left(\frac{-\text{Im}(h_{1-1-1}r_{1d})}{|h_{1-1-1}r_{1d}|}\right). \tag{B13}$$

Here the subscript $d$ denotes $x$, $y$, or $z$, while Im denotes the imaginary part of the concerned argument. Expressions for $h_{jkl}$ and $r_{jd}$ are given in Appendix C. For the instability region where quintic (or septic) TDGL equation holds, an expansion of $\Psi$ up to $\psi_j^{(4)}$ (or up to $\psi_j^{(6)}$) will be required in determining $\vec{R}$, so that

$$\vec{R}=\sum_{n=2}^{N}\epsilon^{n/2}\psi_0^{(n)}e^{\lambda_o\tau}\vec{r}_0+\sum_{n=1}^{N}[\epsilon^{n/2}\psi^{(n)}e^{i\omega\tau}\vec{r}+\text{c.c.}] \tag{B14}$$

with $N=4$ (quintic case) or 6 (septic case). The same procedure as done for the cubic case follows for the quintic as well as the septic cases.

## APPENDIX C

In this appendix we first give the expressions for $h_{kl,j}$, $t_{klm,j}$, $u_{klmn,j}$, $v_{klmnp,j}$, and $w_{klmnpq,j}$ that appear as coefficients in the determination of $\psi_j^{(2)}$, $\psi_j^{(3)}$, $\psi_j^{(4)}$, $\psi^{(5)}$, and $\psi^{(6)}$, respectively, such that

$$\psi_j^{(2)} e^{\lambda_j \tau} = \sum_{l \le k} h_{jkl} \psi_k^{(1)} \psi_l^{(1)} e^{(\lambda_k + \lambda_l)\tau}, \tag{C1}$$

$$\psi_j^{(3)} e^{\lambda_j \tau} = \sum_{m \le l \le k} t_{jklm} \psi_k^{(1)} \psi_l^{(1)} \psi_m^{(1)} e^{(\lambda_k + \lambda_l + \lambda_m)\tau}, \tag{C2}$$

$$\psi_j^{(4)} e^{\lambda_j \tau} = \sum_{n \le m \le l \le k} u_{jklmn} \psi_k^{(1)} \psi_l^{(1)} \psi_m^{(1)} \psi_n^{(1)} e^{(\lambda_k + \lambda_l + \lambda_m + \lambda_n)\tau}, \tag{C3}$$

$$\psi_j^{(5)} e^{\lambda_j \tau} = \sum_{p \le n \le m \le l \le k} v_{jklmnp} \times \psi_k^{(1)} \psi_l^{(1)} \psi_m^{(1)} \psi_n^{(1)} \psi_p^{(1)} e^{(\lambda_k + \lambda_l + \lambda_m + \lambda_n + \lambda_p)\tau}, \tag{C4}$$

and

$$\psi_j^{(6)} e^{\lambda_j \tau} = \sum_{q \le p \le n \le m \le l \le k} w_{jklmnpq} \times \psi_k^{(1)} \psi_l^{(1)} \psi_m^{(1)} \psi_n^{(1)} \psi_p^{(1)} \psi_q^{(1)} \times e^{(\lambda_k + \lambda_l + \lambda_m + \lambda_n + \lambda_p + \lambda_q)\tau}. \tag{C5}$$

We give only those coefficients that contribute to the asymptotic solution. Note that summation over latin alphabets take values 1, 0 and -1 while summation over Greek alphabets take values $\pm 1$:

$$h_{j\alpha\beta} = \frac{g_{j\alpha\beta}}{\lambda_\alpha + \lambda_\beta - \lambda_j}, \tag{C6}$$

$$t_{j\alpha\beta\gamma} = \frac{1}{C_{j\alpha\beta\gamma}} \sum_{l \le \alpha \le k} (g_{j\alpha l} h_{l\beta\gamma} + g_{jk\alpha} h_{k\beta\gamma}), \tag{C7}$$

provided $\alpha + \beta + \gamma \neq j$. Otherwise, $t_{j\alpha\beta\gamma} = 0$. $C_{j\alpha\beta\gamma} = \lambda_\alpha + \lambda_\beta + \lambda_\gamma - \lambda_j$,

$$u_{j\alpha\beta\gamma\delta} = \frac{1}{C_{j\alpha\beta\gamma\delta}} \sum_{k,l} [(g_{j\alpha l} t_{l\beta\gamma\delta} + g_{jk\alpha} t_{k\beta\gamma\delta}) + g_{jkl}(h_{k\alpha\beta} h_{l\gamma\delta})], \tag{C8}$$

where $C_{j\alpha\beta\gamma\delta} = 1/(\lambda_\alpha + \lambda_\beta + \lambda_\gamma - \lambda_j)$:

$$v_{j\alpha\beta\gamma\delta\zeta} = \frac{1}{C_{j\alpha\beta\gamma\delta\zeta}} \sum_{k,l} [(g_{j\alpha l} u_{l\beta\gamma\delta\zeta} + g_{jk\alpha} u_{k\beta\gamma\delta\zeta}) + g_{jkl}(h_{k\alpha\beta} t_{l\gamma\delta\zeta} + h_{l\alpha\beta} t_{k\gamma\delta\zeta})], \tag{C9}$$

provided $\alpha + \beta + \gamma + \delta + \zeta \neq j$. Otherwise, $v_{j\alpha\beta\gamma\delta\zeta} = 0$. The expression $C_{j\alpha\beta\gamma\delta\zeta} = 1/(\lambda_\alpha + \lambda_\beta + \lambda_\gamma + \lambda_\delta + \lambda_\zeta - \lambda_j)$,

$$w_{j\alpha\beta\gamma\delta\zeta\rho} = \frac{1}{C_{j\alpha\beta\gamma\delta\zeta\rho}} \sum_{k,l} [Q + g_{jkl}(h_{k\alpha\beta} u_{l\gamma\delta\zeta\rho} + h_{l\alpha\beta} u_{k\gamma\delta\zeta\rho}) + g_{jkl} t_{k\alpha\beta\gamma} t_{l\delta\zeta\rho}], \tag{C10}$$

where $Q = (g_{j\alpha l} v_{l\beta\gamma\delta\zeta\rho} + g_{jk\alpha} v_{k\beta\gamma\delta\zeta\rho})$ and $C_{j\alpha\beta\gamma\delta\zeta\rho} = 1/(\lambda_\alpha + \lambda_\beta + \lambda_\gamma + \lambda_\delta + \lambda_\zeta + \lambda_\rho - \lambda_j)$.

Next we give the expressions for $\mu_{jk}$, $\eta_j$, and $g_{jkl}$:

$$\mu_{jk} = \frac{c_0 s_{jz}(-r_{kx} + r_{kz})}{\vec{s}_j^T \vec{r}_j}, \tag{C11}$$

$$\eta_j = \sum_{l \le \alpha \le k,\, \gamma \le \beta} (g_{jk\alpha} h_{k\beta\gamma} + g_{j\alpha l} h_{l\beta\gamma}), \tag{C12}$$

$$\text{for} \quad k \neq l, \quad g_{jkl} = 2 f_{xxj} r_{kx} r_{lx} + f_{xyj}(r_{kx} r_{ly} + r_{ky} r_{lx}), \tag{C13}$$

while

$$g_{jkk} = f_{xxj} r_{kx}^2 + f_{xyj} r_{kx} r_{ky}, \tag{C14}$$

where

$$f_{xxj} = \frac{b_0(-s_{jx} + b_0 s_{jy})}{\vec{s}_j^T \vec{r}_j}, \tag{C15}$$

$$f_{xyj} = \frac{-(s_{jx} + b_0 s_{jy})}{\vec{s}_j^T \vec{r}_j}, \tag{C16}$$

$$\vec{r}_j^T = (r_{jx}\ r_{jy}\ r_{jz}), \tag{C17}$$

$$\vec{s}_j^T = (s_{jx}\ s_{jy}\ s_{jz}), \tag{C18}$$

$$\vec{s}_j^T \vec{r}_j = s_{jx} r_{jx} + s_{jy} r_{jy} + s_{jz} r_{jz}, \tag{C19}$$

$$r_{jx} = \chi(c_0 + \lambda_j), \tag{C20}$$

$$r_{jy} = -(c_0 + \lambda_j)(\alpha + \lambda_j), \tag{C21}$$

$$r_{jz} = c_0 \chi, \tag{C22}$$

$$s_{jx} = -(c_0 + \lambda_j)(b_0 \delta + \lambda_j), \tag{C23}$$

$$s_{jy} = r_{jx}, \tag{C24}$$

and

$$s_{jz} = a b_0 \chi. \tag{C25}$$

[1] B. J. Brindley and P. J. Worthington, Metall. Rev. **145**, 101 (1970).
[2] S. R. Bodner and A. Rosen, J. Mech. Phys. Solids **15**, 63 (1967); P. Penning, Acta Metall. **20**, 1169 (1972).
[3] K. Chihab, Y. Estrin, L. P. Kubin, and J. Vergnol, Scr. Metall. **21**, 203 (1987).
[4] E. O. Hall, *Yield Point Phenomena in Metals and Alloys* (Macmillan, London, 1970); J. D. Lubahn and R. P. Felgar, *Plasticity and Creep of Metals* (Wiley, New York, 1961).
[5] T. L. Da Silveria and S. N. Monteiro, Metall. Trans. A **10**, 1795 (1979); L. N. Zagorukuyko, A. I. Osetskiy, and U. P. Soldatov, Phys. Met. Metallogr. **43**, 156 (1977).
[6] V. Stejskalova, M. Hammersky, P. Luckac, P. Vostry, and B. Spuril, Czech. J. Phys., Sect. B **31**, 195 (1981).
[7] A. H. Cottrell, Philos. Mag. **44**, 829 (1953).
[8] P. G. McCormick, Acta Metall. **20**, 351 (1972).
[9] Y. Estrin and L. P. Kubin, J. Mech. Behavior Mater. **2**, 255 (1989); L. P. Kubin and Y. Estrin, Acta Metall. **38**, 697 (1990).
[10] See, for instance, several articles in *Non Linear Phenomena in Materials Science I*, edited by L. P. Kubin and G. Martin (Trans Tech, Zürich, 1988), and references therein.
[11] *Non Linear Phenomena in Materials Science II*, edited by G. Martin and L.P. Kubin (Trans Tech, Zürich, 1992), and references therein. See also the articles in the same volume as Ref. [16].
[12] G. Ananthakrishna and D. Sahoo, J. Phys. D **14**, 2081 (1981); M. C. Valsakumar and G. Ananthakrishna, *ibid.* **16**, 1055 (1983).
[13] G. Ananthakrishna and M. C. Valsakumar, J. Phys. D **15**, L171 (1982).
[14] G. Ananthakrishna and M. C. Valsakumar, Phys. Lett. A **95**, 69 (1983); G. Ananthakrishna, in *Non Linear Phenomena in Materials Science I* (Ref. [10]) and *Non Linear Phenomena in Materials Science II* (Ref. [11]).
[15] G. Ananthakrishna and T. M. John, in *Directions in Chaos*, edited by Hao Bai-lin (World Scientific, Singapore, 1990), Vol. 3, p. 133.
[16] G. Ananthakrishna, Scr. Metall. **29**, 1185 (1993).
[17] G. Ananthakrishna *et al.*, Scr. Metall. **32**, 1731 (1995).
[18] G. Ananthakrishna and S. J. Noronha, in *Non Linear Phenomena in Materials Science III*, edited by G. Ananthakrishna, L. P. Kubin, and G. Martin (Scitec, Zürich, 1995), p. 277; see also L. Quaouire and C. Fressengeas, *ibid.*, p. 293.
[19] S. Venkadesan, M. C. Valskumar, K. P. N. Murthy, and S. Rajasekar, Phys. Rev. E **54**, 611 (1996).
[20] S. J. Noronha, G. Ananthakrishna, L. Quaouire, C. Fressengeas, and L. P. Kubin, Int. J. Bifurcation Chaos Appl. Sci. Eng. (to be published); S. J. Noronha, G. Ananthakrishna, L. Quaouire, and C. Fressengeas, Pramana J. Phys. **48**, 705 (1997).
[21] G. Nicolis and I. Prigogine, *Self Organization in Nonequilibrium Systems* (Wiley, New York, 1977).
[22] H. Haken, *Advanced Synergetics: Instability Hierarchies of Self-Organizing Systems and Devices* (Springer-Verlag, Berlin, 1983).
[23] G. Ananthakrishna and D. Sahoo, J. Phys. D **14**, 699 (1981).
[24] G. Ananthakrishna and D. Sahoo, J. Phys. D **15**, 1439 (1982).
[25] See, for example, E. Aifantis, in *Non Linear Phenomena in Materials Science I* (Ref. [10]). See also P. Hahner and L. P. Kubin *ibid.*; P. Hahner, Mater. Sci. Eng. **164**, 23 (1993).
[26] Mulugeta Bekele and G. Ananthakrishna, Int. J. Bifurcation Chaos Appl. Sci. Eng. (to be published).
[27] T. Taniuti and C. C. Wei, J. Phys. Soc. Jpn. **24**, 941 (1968).
[28] A. C. Newell and J. A. Whitehead, J. Fluid Mech. **38**, 279 (1968).
[29] Y. Kuramoto and T. Tsuzuki, Prog. Theor. Phys. **52**, 1399 (1974).
[30] H. Mashiyama, A. Ito, and T. Ohta, Prog. Theor. Phys. **54**, 1050 (1975).
[31] P. H. Richter, I. Procaccia, and J. Ross, in *Advances in Chemical Physics*, edited by I. Prigogine and S. Rice (Wiley-Interscience, New York, 1981).
[32] L. Y. Chen, N. Goldenfeld, and Y. Oono, Phys. Rev. E **54**, 376 (1996).
[33] J. Carr, *Applications of Center Manifold Theory* (Springer-Verlag, Berlin, 1981).
[34] J. Guckenheimer and P. Holmes, *Nonlinear Oscillations, Dynamical Systems and Bifurcations of Vector Fields Applied Mathematical Sciences*, Vol. 42 (Springer-Verlag, Berlin, 1983).
[35] H. Troger and A. Steindl, *Nonlinear Stability and Bifurcation Theory* (Springer-Verlag, Wien, NY, 1991).
[36] N. Goldenfeld, O. Martin, and Y. Oono, J. Sci. Comput. **4**, 355 (1989).
[37] T. Kunihiro, Prog. Theor. Phys. **94**, 503 (1995); **97**, 179 (1997).
[38] J. D. Murray, J. Chem. Phys. **61**, 3160 (1974).
[39] H. Alexander, in *Dislocations in Solids*, edited by F. R. N. Nabarro (North-Holland, Amsterdam, 1986), p. 151.
[40] L. P. Kubin and Y. Estrin (organizers), Scr. Metall. **29**, 1147 (1993).